Photoelectrical properties and the electronic structure of $Tl_{1-x}In_{1-x}Sn_xSe_2$ (x = 0, 0.1, 0.2, 0.25) single crystalline alloys

G. E. Davydyuk,[a] O. Y. Khyzhun,[ab] A. H. Reshak,*[cd] H. Kamarudin,[d] G. L. Myronchuk,[a] S. P. Danylchuk,[a] A. O. Fedorchuk,[e] L. V. Piskach,[f] M. Yu. Mozolyuk[f] and O. V. Parasyuk[f]

Photoelectrical properties of $Tl_{1-x}In_{1-x}Sn_xSe_2$ single crystalline alloys (x = 0, 0.1, 0.2, 0.25) grown using the Bridgman–Stockbarger method were studied. The temperature dependence of electrical and photoconductivity for the $Tl_{1-x}In_{1-x}Sn_xSe_2$ single crystals was explored. It has been established that photosensitivity of the $Tl_{1-x}In_{1-x}Sn_xSe_2$ single crystals increases with x. The spectral distribution of photocurrent in the wavelength spectral range 400–1000 nm has been investigated at various temperatures. Photoconductivity increases in all the studied crystals with temperature. Therefore, thermal activation of photoconductivity is caused by re-charging of the photoactive centers as the samples are heated. Based on our investigations, a model of center re-charging is proposed that explains the observed phenomena. X-ray photoelectron valence-band spectra for pristine and Ar^+-ion irradiated surfaces of the $Tl_{1-x}In_{1-x}Sn_xSe_2$ single crystals have been measured. These results reveal that the $Tl_{1-x}In_{1-x}Sn_xSe_2$ single-crystal surface is sensitive to the Ar^+ ion irradiation that induced structural modification in the top surface layers. Comparison on a common energy scale of the X-ray emission Se $K\beta_2$ bands representing energy distribution of the Se 4p-like states and the X-ray photoelectron valence-band spectra was done.

1. Introduction

$TlInSe_2$ belongs to a class of semiconductor compounds with layered structures; it has an indirect optical band gap ($E_g \sim 1.4$ eV) at room temperature and is considered to be a potential material for optoelectronics.[1] It also features a high thermoelectric figure of merit, large gauge factors, high photosensitivity, and good memory switching properties.[2,3] A number of papers report the investigation of the solid solutions based on the compounds of this family (see, *e.g.*, ref. 1, 3 and 4), because of tuning of properties of materials within the homogeneity regions. We have recently discovered during the study of the $TlInSe_2$–$SnSe_2$ phase diagram[5] the formation of a large solid solubility region of thallium indium diselenide which extends from 0–28 mol% $SnSe_2$ at 670 K. XRD studies determined that within the solid solution range, tin atoms which occupy octahedral voids in the $SnSe_2$ structure[6] (Fig. 1) with the inter-atomic distances Sn–Se = 0.2680 nm are located in the tetrahedral voids (crystallographic site 4b) in a statistical mix with indium atoms (Fig. 2), with somewhat shorter distances to selenium atoms.[5,7] The 4a site in which thallium atoms are located becomes partially occupied due to the subtraction of these atoms with the increase of tin diselenide content. The packing of cation-centered tetrahedral of the statistical mix In + Sn and of the tetragonal antiprisms around Tl atoms is shown in Fig. 2. A small addition of tin atoms ($TlIn_{0.99}Sn_{0.01}Se_2$) leads to a significant increase of tensosensitivity compared to pure $TlInSe_2$.[8] We have studied in ref. 9 optical properties of samples in the entire concentration range of the $Tl_{1-x}In_{1-x}Sn_xSe_2$ solid solutions (x = 0–0.25), including two-photon absorption at 9.4 μm wavelength and at various temperatures.

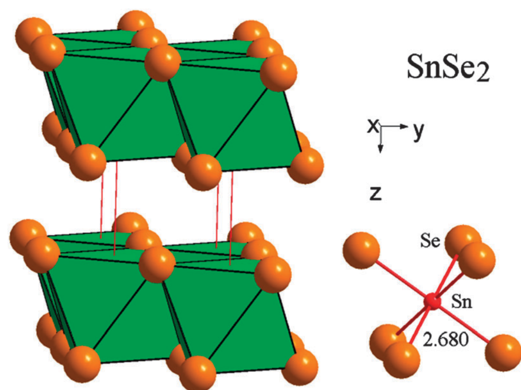

Fig. 1 Packing of the octahedra of selenium atoms and inter-atomic distances of the anion–cation in the $SnSe_2$ structure.

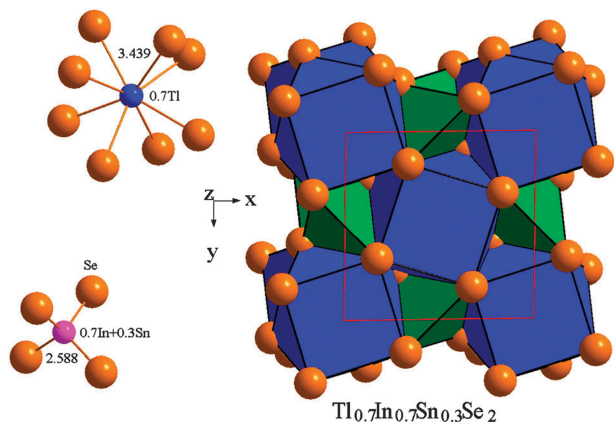

Fig. 2 Packing of the polyhedra of selenium atoms around cation atoms and inter-atomic distances within these polyhedra in the structure of alloys within the $Tl_{1-x}In_{1-x}Sn_xSe_2$ solid solutions.

In addition, the above-mentioned samples have been tested in ref. 9 employing X-ray photoelectron spectroscopy (XPS) by measuring core-level binding energies of the atoms constituting the solid solutions under consideration.

Here we present the results of an investigation of the temperature dependence of electrical and photoconductivity of the single crystals $Tl_{1-x}In_{1-x}Sn_xSe_2$ (x = 0, 0.1, 0.2, 0.25) grown using the Bridgman–Stockbarger method, as well as data of measurements of XPS valence-band spectra for pristine and Ar^+-ion irradiated surfaces of the single crystals under consideration. Since in a number of experimental studies and first-principles band-structure calculations of binary, ternary and quaternary di- and tetraselenides (sulfides) it has been established (see, *e.g.*, ref. 10–15) that their electronic structure is characterized by significant contributions of the valence Se p (S p) states throughout the whole valence band region, in the present paper we have measured for the $Tl_{1-x}In_{1-x}Sn_xSe_2$ single crystals (x = 0.1, 0.2, 0.25) the X-ray emission Se $K\beta_2$ bands representing energy distribution of the Se 4p-like states and compared them on a common energy scale with the XPS valence-band spectra.

In Section 2 is presented information concerning the crystal growth. The applied experimental methods are given in Section 3. Experimental results of thermo- and photoelectrical properties and their origin following the band structure analysis are given in Section 4.

2. Single crystal growth

Single crystals of the solid solution $Tl_{1-x}In_{1-x}Sn_xSe_2$, where x = 0, 0.1, 0.2, 0.25, were grown using the Bridgman–Stockbarger method. The crystals were synthesized and grown in quartz ampoules with a conical bottom. Calculated amounts of high-purity elements (at least 99.999 wt%) were soldered in evacuated ampoules and placed in a single-zone furnace upside down. After heating to 80–100 K above the liquidus (according to the phase diagram[5]) they were held at this temperature for 12 h using periodic vibration. After cooling to room temperature, the ampoules were transferred to the pre-heated two-zone growth furnaces. The growth process consisted of the gradual crystallization onto the formed and annealed seed at the rate of 7 mm per day with the temperature gradient at the solid–melt interface of 3–3.5 K mm^{-1}. Obtained crystals were annealed for 100 h at 720–770 K, and then cooled to room temperature during another 100 h. As-grown single-crystalline boules were up to 30 mm in length and up to 9 mm in diameter. A typical boule is presented in Fig. 3a. The single crystals cleave easily along the cleavage plane forming a mirror surface (Fig. 3b) that does not require additional processing for further investigations.

3. Experimental

Investigation of the temperature dependence of conductivity and photoconductivity was performed on the samples prepared from the single crystals by cleaving along the cleavage planes. The crystal surfaces were mirror-smooth and did not require any additional treatment for the measurement. Ohmic contacts were prepared by melting indium onto the opposite surfaces.

Photoelectric measurements were performed by standard techniques using an MDR-206 monochromator in the temperature range of 150–300 K with a spectral resolution of 0.8 nm. Temperature was controlled using a UTRECS K41 thermoregulator with $\pm$0.1 K accuracy. The current was measured using a Keithley 6514 electrometer.

XPS valence-band spectra for the as-grown $Tl_{1-x}In_{1-x}Sn_xSe_2$ (x = 0.1, 0.2, and 0.25) single crystals were measured using an ion-pumped chamber having a base pressure less than 3×10^{-10} mbar of the UHV-Analysis-System assembled by SPECS Surface Nano Analysis Company (Berlin, Germany). The system is equipped with a PHOIBOS 150 hemispherical analyser. The spectra were excited by a Mg Kα source of X-ray irradiation (E = 1253.6 eV) and were recorded at a constant pass energy of 30 eV. The energy scale of the spectrometer was calibrated as reported in ref. 15. The $Tl_{1-x}In_{1-x}Sn_xSe_2$ single crystal samples for the present XPS measurements were prepared in the shape of thin plates with the following dimensions: length $\sim$7 mm, width $\sim$5–6 mm, and height $\sim$1–1.5 mm. The plates were polished with castor oil containing additions of beryllium abrasive no. 28 to gain high-quality optical surfaces following

Fig. 3 Panoramic view of the as-grown (a) $Tl_{0.8}In_{0.8}Sn_{0.2}Se_2$ and (b) $Tl_{0.9}In_{0.9}Sn_{0.1}Se_2$ single crystals.

the technique reported in ref. 16. The charging effects were taken into account in reference to the C 1s line (284.6 eV) of adventitious carbon as suggested for such types of materials.[17] With the aim of removing surface contaminations, bombardment of the crystal surface has been made with Ar^+ ions with an energy of 3.0 keV for 5 min at an ion current density of 14 μA cm^{-2}. The total Ar^+ flux was $\sim$5.3 × 10^{16} ions per cm^2. The fluorescent X-ray emission (XE) Se Kβ_2 band (K → $N_{II,III}$ transition), which represents the energy distribution of the valence Se p-like states, in the $Tl_{1-x}In_{1-x}Sn_xSe_2$ single crystals was recorded in the third order of reflection using a Johann-type DRS-2M spectrograph equipped with an X-ray BHV-7 tube (gold anode) using the technique described in ref. 18. As a disperse element, a quartz crystal with the (0001) reflecting plane was used. The XE Se Kβ_2 band was measured with the spectrograph energy resolution of about 0.3 eV.

4. Results and discussion

4.1. Thermoelectric properties

The $Tl_{1-x}In_{1-x}Sn_xSe_2$ crystals (x = 0–0.25) are typical representatives of the layered semiconductors of the $A^{III}B^{III}C^{VI}{}_2$ group characterized by numerous structural defects such as vacancies and dislocations. If the concentration of these defects is high, energy levels within the band gap form a band of localized defect states which pin the Fermi level between the occupied and empty states. High density of states localized near the Fermi level are responsible for the majority of electrical processes occurring in semiconductors.[19]

All the obtained crystals, regardless of x, are high-resistance materials of p-type conductivity according to the sign of the thermo-EMF coefficient. Hole conductivity may be caused by the acceptor nature of the stoichiometric cation vacancies with deep energy levels in the lower half of the band gap which is typical of many complex chalcogenide semiconductor compounds. Invariability of the conductivity type upon the increase of x, accompanied by the substitution of Sn for In (the formation of donor centers), indicates that the concentration of dopant Sn atoms is lower than the concentration of stoichiometric vacancies and other structural defects.

High concentration of stoichiometric vacancies may promote the structure-sensitive ionic conductivity caused by the mobility of metal ions by the empty sites of the crystal lattice. Ionic conductivity is minor compared to the electron component at low temperature due to low ion mobility and high activation energy. The study of ionic conductivity in the solid solutions of $TlInSe_2$ and $TlInTe_2$ was reported in ref. 20, where the authors showed that the electron component of conductivity is dominant below T^{II} = 391 K and $T^{\perp}$ = 388 K. Further increase of temperature results in the jump in conductivity related to the growth of the ionic component caused by the disordering of the cation sub-lattice of Tl^+. In this temperature region the ionic conductivity of the crystals outweighs the electron component. In this work the investigation of electrical and photoelectrical parameters was performed at room temperature and below, with short-term switching of the power source to the sample (to decrease the polarization effects). Under these conditions the results of the investigation are determined by the electron component of conductivity that prevails over the ionic one, as was experimentally observed.

High V_{Tl} concentration resulting from the incomplete occupation of the 4a site with Tl atoms as well as the statistical nature of the substitution of Sn atoms for In atoms in the 4b site[5] and the presence of other defects are some of the reasons for the deviation from the long-range order of the location of atoms in the crystal.[19] This leads to the appearance of additional energy states in the band gap thus approximating the investigated crystals as the disordered systems. Physical properties of the disordered systems have a series of peculiarities, *e.g.* in optical spectra, this shows as the Urbach's edge of the fundamental transitions. In the charge transfer processes, temperature dependence of conductivity $\sigma(T)$ may be extrapolated in the coordinate system $\ln\sigma - 1/T$ by several straight lines with various activation energies E_A that correspond to different transfer mechanisms.[21]

Temperature dependence of the specific dark conductivity of the crystals in various temperature ranges fits well the law typical of the disordered semiconductors:[19,21]

$$\sigma(T) = \sigma_0 \exp(-E_A/kT), \quad (1)$$

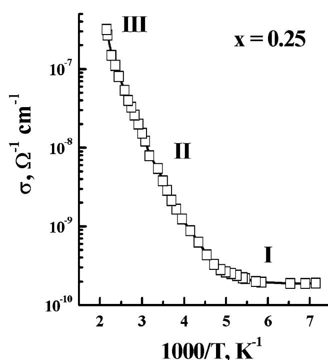

Fig. 4 Temperature dependence of the specific dark conductivity of the $Tl_{0.75}In_{0.75}Sn_{0.25}Se_2$ crystal.

where the pre-exponent factor σ_0 depends on the conductivity mechanism.[21] The values of $\sigma_0 = 10^2$–$10^4\ \Omega^{-1}\ cm^{-1}$ correspond to the excitation of holes from the states near the Fermi level in the band gap to the non-localized states in the valence band (for p-type); $\sigma_0 = 10^{-2}$–$1\ \Omega^{-1}\ cm^{-1}$ is related to the excitation of the carriers from the states near E_F to the localized states in the tail of the valence band; the values of $\sigma_0 \ll 10^{-2}\ \Omega^{-1}\ cm^{-1}$ are explained by the thermally activated jump conductivity in the band of localized defect states near E_F.

Temperature dependence of the specific dark conductivity of the $Tl_{1-x}In_{1-x}Sn_xSe_2$ crystal with $x = 0.25$ is shown in Fig. 4. Similar temperature dependence is observed for the samples with $x = 0.10$ and $x = 0.20$. It is necessary to emphasize that we deal with intrinsic defect states and these states form an effective electron density states below the conduction band.

Activation energy in the low-temperature region I of $\sigma(T)$ equals E_{A1} = 0.18 eV, 0.17 eV, 0.15 eV for various samples (Table 1) with the pre-exponent factor $\sigma_0 \sim 10^{-6}\ \Omega^{-1}\ cm^{-1}$. Such parameters are typical of the conductivity within the impurity defect band caused by the thermally activated jumps of carriers between the localized states near the Fermi level in this band. The activation energy of such jumps is close to the half-width of the defect band of the localized states in which E_F is located ($\Delta E \approx 2\,E_A$). In our case $\Delta E \sim 0.3$ eV which is close to the ΔE values of amorphous semiconductors.[19]

Activation energy E_{A2} in the temperature region II equals 0.49 eV, 0.44 eV, 0.43 eV for the above-mentioned samples, with σ_0 increasing to 2–20 $\Omega^{-1}\ cm^{-1}$, which is common in disordered systems for the electron transitions from the defect band of the localized states crossing the Fermi level to the localized states in the tail of the valence band.

Activation energy E_{A3} in the high-temperature region III ($T > 400$ K) equals 1.04 eV, 1.24 eV, and 1.29 eV for x = 0.10, 0.20, and 0.25, respectively. As σ_0 has a value of $\sim 10^4\ \Omega^{-1}\ cm^{-1}$, this corresponds according to Mott's criterion to the conductivity mechanism of the excitation of holes from the states near E_F in the band of the localized states to the non-localized states in the valence band. In this case the value of E_{A3} equals the energy distance of E_F to the level of the valence band energy position. The position of the Fermi level in a partially compensated semiconductor depends on the energy level of donors and acceptors and the ratio of their concentration. In the $Tl_{1-x}In_{1-x}Sn_xSe_2$ solid solutions, the increase of Sn concentration (*i.e.*, x) is accompanied by the substitution of Sn atoms for In atoms with the formation of Sn_{In} centers (donors). Meanwhile the same amount of V_{Tl} (acceptors) is formed, thus preserving the ratio of the concentration of the compensating centers without the change in their nature. This means that the position of the Fermi level in the band gap should not change with x. Experimental results show the increase of E_{A3} with x which determines the position of the Fermi level (Table 1). In our opinion, this is caused by the increase of the band gap E_g with x. This conclusion agrees well with the change in the optical band-gap energy determined from the absorption spectra in the fundamental transition region where the absorption coefficient is described using Urbach's rule.

Table 1 Activation energy of the specific dark conductivity of the $Tl_{1-x}In_{1-x}Sn_xSe_2$ crystals

	x = 0.10	x = 0.20	x = 0.25
E_{A1}, eV (I)	0.18	0.17	0.15
E_{A2}, eV (II)	0.49	0.44	0.43
E_{A3}, eV (III)	1.04	1.24	1.29

4.2. Photoelectric properties

The investigation of photoelectric properties of $TlInSe_2$ and its various solid solutions was reported in ref. 22–24. The $Tl_{1-x}In_{1-x}Sn_xSe_2$ single crystals are also photosensitive materials. The multiple of the photoresponse to the integral light illumination of $L = 10^4$ Lux (σ_l/σ_d where σ_l is the conductivity under illumination, σ_d is the dark conductivity) is presented in Table 2.

Spectral characteristics of photoconductivity of the $Tl_{1-x}In_{1-x}Sn_xSe_2$ single crystals (x = 0.1–0.25) at 300 K are shown in Fig. 5. It was determined that the wide maxima lie in the region of the fundamental transitions and are clearly the intrinsic photoconductivity maxima. Their spectral position is given in Table 3. The change in the position of the photoconductivity maximum with x from λ_m = 745 nm (for x = 0.1) to λ_m = 660 nm (for x = 0.25) results from the change in the band-gap energy which agrees with the optical investigation of E_g performed by the absorption studies in the fundamental transition region (Table 3).

It may be assumed that the increase of photosensitivity with x, *i.e.* the increase of the band-gap energy (Fig. 5), is due to the re-distribution of the recombination flux of holes from s-centers of rapid recombination to r-centers of slow recombination. The role of s-centers is usually played by various structural defects,[25] while cation vacancies (V_{Tl}) act as r-centers. As E_g increases

Table 2 The multiple of the photoresponse of the $Tl_{1-x}In_{1-x}Sn_xSe_2$ crystals at 300 K

	x = 0	x = 0.10	x = 0.20	x = 0.25
σ_l/σ_d	1.02	1.1	1.3	1.9

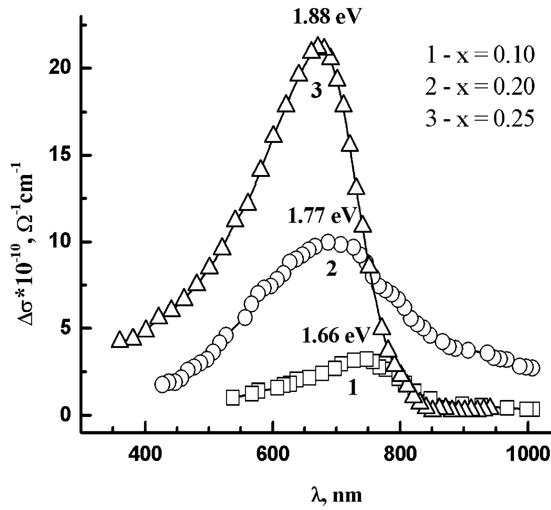

Fig. 5 Spectral distribution of photoconductivity of the $Tl_{1-x}In_{1-x}Sn_xSe_2$ crystals at 300 K.

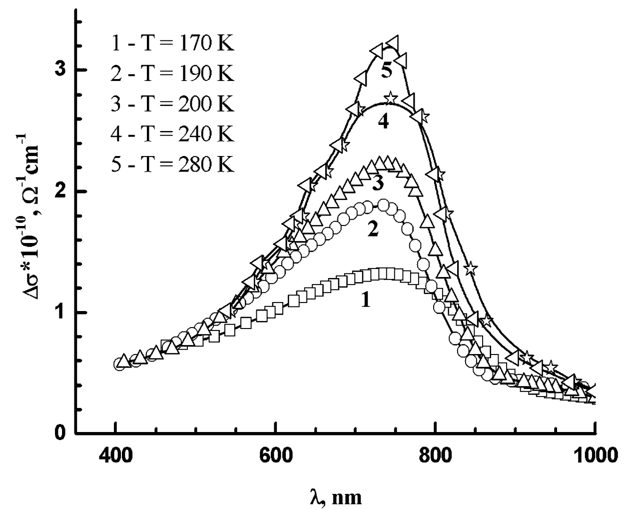

Fig. 6 Spectral distribution of photoconductivity of the $Tl_{0.90}In_{0.90}Sn_{0.10}Se_2$ single crystal.

Table 3 Maximum of intrinsic photoconductivity (E_M) and band-gap energy (E_g) determined from the absorption spectra in the fundamental transition region of the $Tl_{1-x}In_{1-x}Sn_xSe_2$ crystals

	x = 0.10	x = 0.20	x = 0.25
E_M, eV	1.66	1.79	1.88
E_g, eV	1.68	1.83	1.87

within the solid solution range, the distance between the Fermi level and the levels of s- and r-centers may change which would thus affect their occupation with carriers and, consequently, the recombination flux through these centers.

The spectral distribution of photocurrent in the wavelength range 400–1000 nm was investigated at various temperatures (Fig. 6–8). Photoconductivity increases in all studied crystals with temperature, which indicates thermal activation of photoconductivity (TAP) that is related to the re-charging of the photoactive centers as the samples are heated.

Temperature dependence of the photosensitivity of the $Tl_{1-x}In_{1-x}Sn_xSe_2$ single crystals of various compositions is presented in Fig. 9. The photosensitivity of the single crystals of the solid solution increases with temperature and with the band-gap energy. The increase of E_T (TAP activation energy) accompanies the process.

Based on our investigations, a model of center re-charging is proposed that explains observed phenomena and does not contradict the experimental results.

Complex semiconductor compounds to which group our crystals belong have a wide spectrum of structural defects, some of which act as slow recombination centers (r-centers), others are rapid recombination centers (s-centers), and traps, or trapping levels (t-centers) for the free carriers in the bands.

We assume that t-centers are bound to the valence band, *i.e.* they do not change their position relative to the valence band. Such centers are often observed in semiconductors.[26] In that

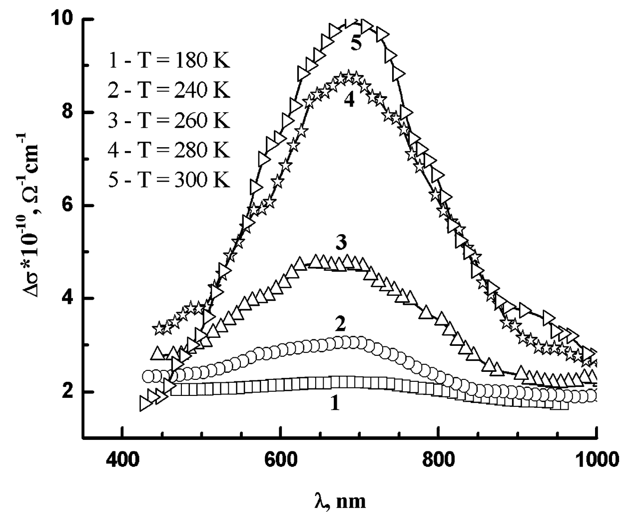

Fig. 7 Spectral distribution of photoconductivity of the $Tl_{0.80}In_{0.80}Sn_{0.20}Se_2$ single crystal.

case, the increase of E_g is accompanied by the increase of the energy level of t-centers (E_T) relative to the conduction band.

The t-centers may act as both the trapping levels for electrons and the recombination centers (depending on E_T and temperature). If the rate of the thermal excitation of electrons trapped at t-centers back to the conduction band is higher than the rate of their recombination with the holes of the valence band, they act as traps:[27]

$$n_t v S_n N_C e^{-\frac{E_T}{kT}} > n_t v S_p p \quad (2)$$

where n_t is the concentration of electrons trapped at t-centers; v is the speed of free charge carriers in the bands; S_n is the section of electron trapping by a t-center from the conduction band; S_p is the section of hole trapping by a t-center; p is the concentration of holes in the valence band; N_C is the density of the electron states at the bottom of the conduction band.

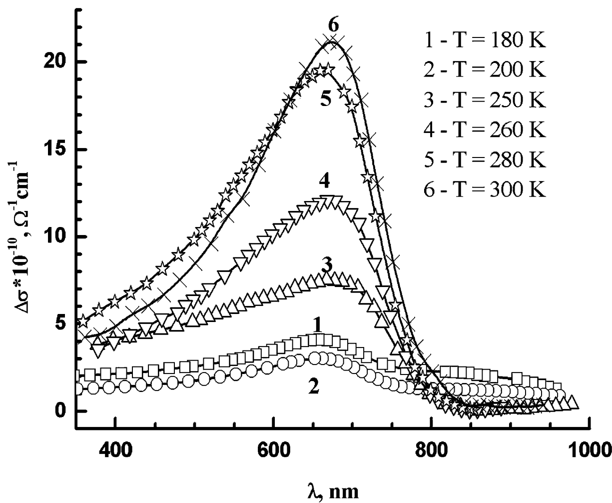

Fig. 8 Spectral distribution of photoconductivity of the $Tl_{0.75}In_{0.75}Sn_{0.25}Se_2$ single crystal.

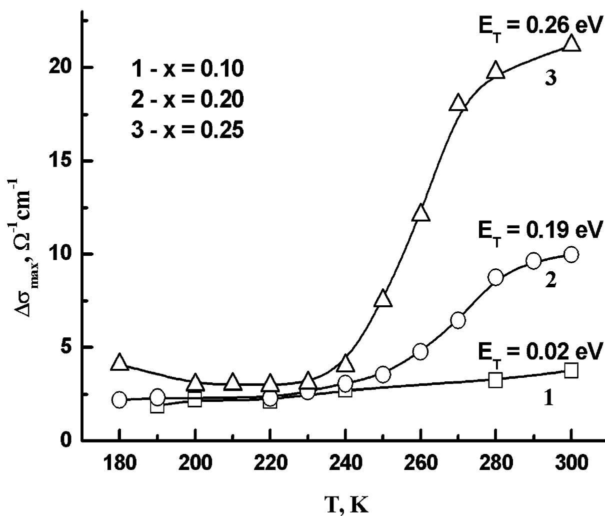

Fig. 9 Temperature dependence of the photoconductivity maxima of the $Tl_{1-x}In_{1-x}Sn_xSe_2$ single crystals.

If the rate of the recombination of the holes and electrons trapped at t-centers is higher than the rate of the thermal excitation of electrons to the conduction band, they act as the recombination centers, and the sign in eqn (2) should be changed to the opposite one:

$$n_t v S_n N_C e^{-\frac{E_T}{kT}} < n_t v S_p p \quad (3)$$

The compounds with low E_T values feature insignificant trapping of electrons excited to the conduction band by the trapping centers, and all electrons recombine with the non-equilibrium holes through r- and s-centers. The occupation of r- and s-centers with electrons reaches maximum, and the lifetime of holes τ_p in the valence band is minimum:

$$\tau_p = 1/vS_p n_c, \quad (4)$$

where S_p is the section of hole trapping by a center in the valence band; n_c is the concentration of electrons at the recombination centers (r- and s-centers).

Photosensitivity is proportional to the mobility of holes μ which we will consider constant for the crystals of various compositions and their lifetime in the valence band:

$$\Delta\sigma \sim \mu\tau \quad (5)$$

The increase of E_T which is observed upon the increase of x and consequently E_g of the solid solution crystal leads to higher efficiency of the trapping centers (formula (2)). This is exhibited in higher occupation of t-centers with electrons and the decrease of their concentration in the conduction band as well as the recombination centers. As a result, τ_p (formula (4)) and the photosensitivity of the sample increase.

At low temperatures (especially for the samples with large x and, respectively, high E_T) the rate of the freeing of electrons from t-centers is lower than the rate of the recombination with holes. Inequality (3) becomes true, and t-centers act as the recombination centers.

In this case the recombination of the non-equilibrium holes with the electrons of the conduction band would utilize three recombination centers (r, s, t) which causes low τ_p values and, consequently, low photosensitivity. At higher temperature the conditions of eqn (3) may change to the conditions of (2) where t-centers act as trapping levels. This decreases the number of the recombination channels (r, s) which leads to higher τ_p and photosensitivity.

Therefore the proposed model of the re-charging of defect centers explains well the increase of the photosensitivity of the investigated crystals at various temperatures with the change in the composition (x) of the crystals.

4.3. Electronic structure

Fig. 10 demonstrates the XPS valence-band spectra (including some upper core-levels) of the $Tl_{1-x}In_{1-x}Sn_xSe_2$ single crystals recorded for their pristine and Ar^+ ion-bombarded surfaces. The influence of middle-energy Ar^+ bombardment on the XPS valence-band spectra of surfaces of the $Tl_{1-x}In_{1-x}Sn_xSe_2$ single crystal solid solutions is very important because this method of surface cleaning is widely applied in epitaxial technologies. From Fig. 10, it is evident that surfaces of the $Tl_{1-x}In_{1-x}Sn_xSe_2$ single crystals are sensitive to the Ar^+ ion-bombardment. As can be seen from Fig. 10, the Ar^+ ion bombardment of $Tl_{1-x}In_{1-x}Sn_xSe_2$ single crystal surfaces with 3.0 keV Ar^+ ions for 5 min decreases somewhat relative content of thallium atoms in the top surface layers. As a result of such a treatment, values of binding energies of the XPS Tl 5d core-level spectra increase somewhat, while binding energies of the XPS In 4d core-level spectra remain constant within the accuracy of the present measurements (±0.05 eV). It is worth mentioning that the present data agree well with the precise XPS core-level measurements of binding energies of atoms constituting the $Tl_{1-x}In_{1-x}Sn_xSe_2$ single crystal surfaces, both pristine and Ar^+ ion-bombarded.[9] As it has been established in ref. 9, Ar^+ ion bombardment of $Tl_{1-x}In_{1-x}Sn_xSe_2$ single-crystal surfaces with 3.0 keV Ar^+ ions for 5 min increases somewhat values of binding

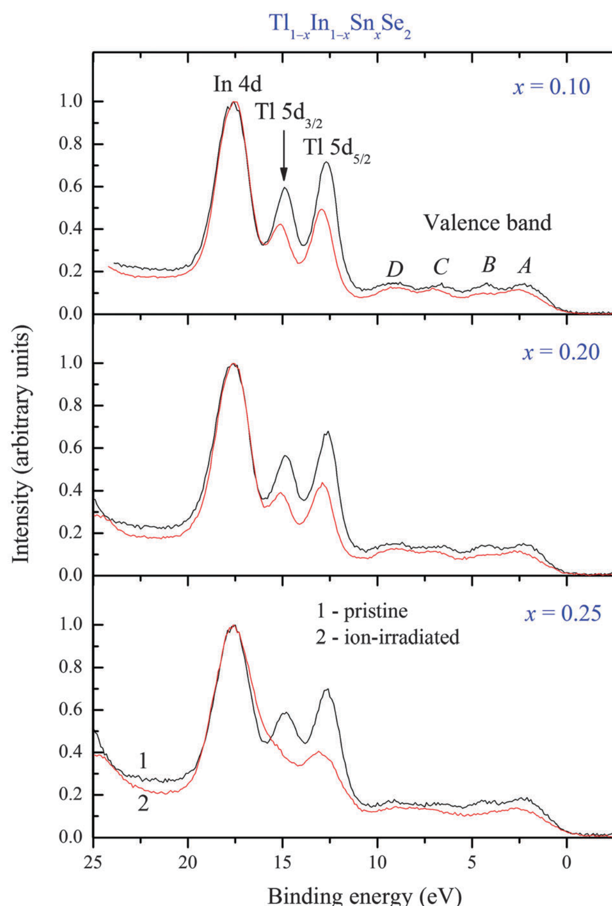

Fig. 10 XPS valence-band spectra (including some upper core-levels) recorded for (1) pristine and (2) Ar^+ ion-bombarded surfaces of the $Tl_{1-x}In_{1-x}Sn_xSe_2$ (x = 0.1, 0.2, and 0.25) single crystals.

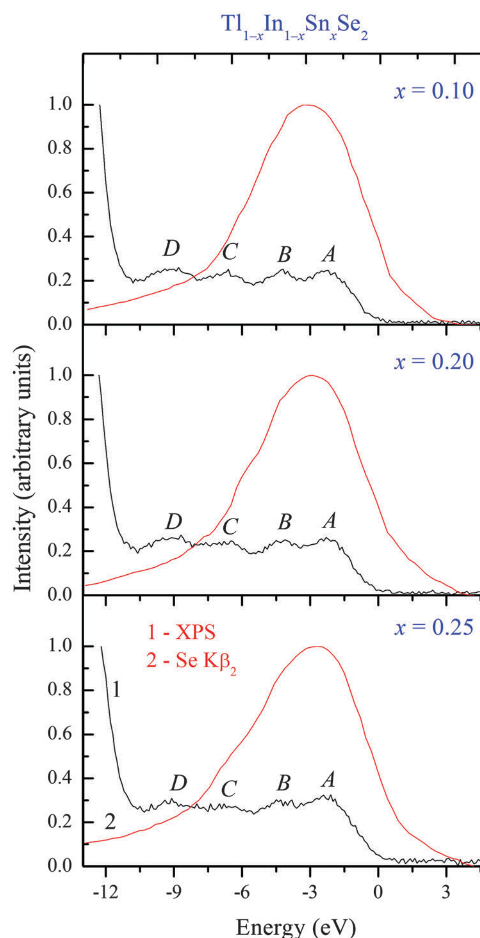

Fig. 11 Comparison on a common energy scale of (1) the XPS valence-band spectra and (2) the X-ray emission Se $K\beta_2$ bands of the $Tl_{1-x}In_{1-x}Sn_xSe_2$ (x = 0.1, 0.2, and 0.25) single crystals.

energies of the XPS Tl 4f core-level spectra, while binding energies of the XPS Sn 3d core-level spectra decrease somewhat as a result of such a treatment. The presented features indicate some degree of overlap of the corresponding localised states with the ligands. Therefore, the $Tl_{1-x}In_{1-x}Sn_xSe_2$ single-crystal surface is sensitive to the Ar^+ ion irradiation that induced structural modifications in the top surface layers. The XPS valence-band spectra reveal four fine-structure peculiarities, namely A, B, C, and D, with binding energies of about 2.3, 4.2, 6.7, and 9.2 eV, respectively, for all pristine surfaces of the single crystals studied. Energy positions of the above fine-structure peculiarities of the XPS valence-band spectra do not change within an accuracy of $\pm$0.1 eV when varying x in the $Tl_{1-x}In_{1-x}Sn_xSe_2$ single crystals under consideration.

Fig. 11 shows the X-ray emission Se $K\beta_2$ bands and XPS valence-band spectra of the $Tl_{1-x}In_{1-x}Sn_xSe_2$ single-crystals provided that a common energy scale is used. The technique of matching the above X-ray emission and photoelectron spectra of the single crystals under study on a common energy scale was similar to that described in ref. 11 and 18 and it is commonly used in experimental XE studies of solids (for details, see, *e.g.*, monographs[28,29]). It is worth mentioning that zero energy of the X-ray emission Se $K\beta_2$ bands and the XPS valence-band spectra presented in Fig. 11 corresponds to the position of the Fermi level of the PHOIBOS 150 hemispherical energy analyzer. The experimental data reveal that main contributions of the Se 4p-like states occur in the upper portion of the valence band, with also significant contributions of the mentioned states throughout the whole valence-band region of the $Tl_{1-x}In_{1-x}Sn_xSe_2$ single crystals. Previously such a conclusion was made when studying a number of ternary and quaternary selenides and sulfides.[10,12–15]

The results obtained may be interpreted within a framework of the band energy structure scheme[30–34] following which the upper valence band was formed by the p-originated anionic states and the conduction band is formed by the s-conduction states. The layered structure usually favours large anisotropy in the transport properties in different directions. For the layered structures, low-dimensional bands begin to play an additional role, giving some flattened bands, which may stimulate the additional charge density and centricity.[35,36]

5. Conclusions

Spectral characteristics of photoconductivity of the $Tl_{1-x}In_{1-x}Sn_xSe_2$ single crystals (x = 0.1–0.25) have shown that the change in the

position of the photoconductivity maximum with x from λ_m = 745 nm (for x = 0.1) to λ_m = 660 nm (for x = 0.25) results from the change in the band-gap energy, E_g, which agrees well with the optical investigation of E_g. The spectral distribution of photocurrent in the spectral wavelength range 400–1000 nm has been studied at various temperatures varying within 170–300 K. These studies clearly demonstrate that photoconductivity of the $Tl_{1-x}In_{1-x}Sn_xSe_2$ single crystals is related to the re-charging of the photoactive centers as the samples are heated. Further, measurements of temperature dependence of the photosensitivity of the $Tl_{1-x}In_{1-x}Sn_xSe_2$ single crystals reveal that their photosensitivity increases with temperature and with the band-gap energy. XPS valence-band measurements of pristine and Ar^+ ion-irradiated surfaces (total Ar^+ flux was fixed at about 5.3×10^{16} ions per cm^2) of the $Tl_{1-x}In_{1-x}Sn_xSe_2$ single crystal solid solutions reveal that their surfaces are sensitive to the Ar^+ ion irradiation inducing structural modification in the top surface layers.

Acknowledgements

A. H. Reshak's work was supported by the Institutional Research Concept of the project CENAKVA (no. CZ.1.05/2.1.00/01.0024), grant no. 152/2010/Z of the Grant Agency of the University of South Bohemia and School of Material Engineering, Malaysia University of Perlis, Malaysia.

References

1 E. Kerimova, S. Mustafaeva, D. Guseinova, I. Efendieva, S. Babaev, T. G. Mamedov, T. S. Mamedov, Z. Salaeva and K. Allakhverdiev, *Phys. Status Solidi A*, 2000, **179**, 199.
2 N. Mamedov, K. Wakita, A. Ashida, T. Matsui and K. Morii, *Thin Solid Films*, 2006, **499**, 275.
3 E. M. Godzhaev and K. D. Gyul'mamedov, *Inorg. Mater.*, 2002, **38**, 1206.
4 M. E. Kerimova, J. G. Guseinov and F. Mamedov, *Turk. J. Phys.*, 1997, **21**, 225.
5 M. Yu. Mozolyuk, L. V. Piskach, A. O. Fedorchuk, I. V. Kityk, I. D. Olekseyuk and O. V. Parasyuk, *J. Alloys Compd.*, 2011, **509**, 2693.
6 B. Palosz and E. Salje, *J. Appl. Crystallogr.*, 1989, **22**, 622.
7 D. Muller, G. Eulenberger and H. Hahn, *Z. Anorg. Allg. Chem.*, 1973, **398**, 207.
8 Zh. D. Ashurov, I. Nuritdinov and S. Kh. Umarov, *Perspektivnyye Materialy*, 2011, **1**, 11 (in Russian).
9 G. E. Davydyuk, O. V. Parasyuk, G. L. Myronchuk, O. Y. Khyzhun, R. A. Andrievski, A. O. Fedorchuk, S. P. Danylchuk, L. V. Piskach, M. Yu. Mozolyuk, N. AlZayed and I. V. Kityk, *Opt. Mater* (in preparation).
10 A. A. Lavrentyev, B. V. Gabrelian, I. Y. Nikiforov, J. J. Rehr and A. L. Ankudinov, *J. Phys. Chem. Solids*, 2003, **64**, 1251.
11 O. Y. Khyzhun, M. V. Karpets and O. K. Sinelnichenko, *Metallofiz. Noveishie Tekhnol.*, 2006, **28**, 1451.
12 A. H. Reshak, S. Auluck, I. V. Kityk, A. Perona and B. Claudet, *J. Phys.: Condens. Matter*, 2008, **20**, 325213.
13 A. A. Lavrentyev, B. V. Gabrelian, I. Y. Nikiforov, O. V. Parasyuk and O. Y. Khyzhun, *J. Alloys Compd.*, 2009, **481**, 28.
14 S.-H. Ma, Z.-Y. Jiao and X.-Z. Zhang, *J. Mater. Sci.*, 2012, **47**, 3849.
15 V. L. Bekenev, V. V. Bozhko, O. V. Parasyuk, G. E. Davydyuk, L. V. Bulatetska, A. O. Fedorchuk, I. V. Kityk and O. Y. Khyzhun, *J. Electron Spectrosc. Relat. Phenom.*, 2012, **185**, 559.
16 A. Y. Tarasova, L. I. Isaenko, V. G. Kesler, V. M. Pashkov, A. P. Yelisseyev, N. M. Denysyuk and O. Y. Khyzhun, *J. Phys. Chem. Solids*, 2012, **73**, 674.
17 O. V. Parasyuk, A. O. Fedorchuk, G. P. Gorgut, O. Y. Khyzhun, A. Woiciechowski and I. V. Kityk, *Opt. Mater.*, 2012, **35**, 65.
18 O. Y. Khyzhun, Y. V. Zaulychny and E. A. Zhurakovsky, *J. Alloys Compd.*, 1996, **244**, 107.
19 V. L. Bonch-Bruevich, N. T. Zvyagin, R. Koiper, A. G. Mironov, R. Enderline and B. Esser, *Electron nature of disordered semiconductors*, Nauka, Moscow, 1981 (in Russian).
20 R. M. Sardarly, O. A. Samedov, A. P. Abdullayev, F. T. Salmanov, O. Z. Alekperov, E. K. Huseynov and N. A. Aliyeva, *Semiconductors*, 2011, **45**, 1387–1390.
21 N. Mott and E. Devis, *Electronical processes in noncrystalline substances*, Mir, Moscow, 1974 (in Russian).
22 A. M. Badr and I. M. Ashraf, *Phys. Scr.*, 2012, **86**, 035704.
23 E. M. Godzhaev and G. S. Dzhafarova, *Neorg. Mater.*, 2009, **45**, 1317.
24 E. M. Kerimova, N. Z. Gasanov, L. A. Ismailzade, A. I. Gasanov, S. F. Bairamov, S. S. Abdinbekov and P. G. Ismailova, *Fizika-riyaziyyat v texnika elmlri seriyası, fizika v astronomiya*, 2009, **5**, 137 (in Russian).
25 V. E. Lashkarev, A. V. Liubchenko and M. K. Sheinkman, *Non-equilibrium Processes in Photoconductors*, Naukova Dumka, Kyiv, 1981.
26 A. M. Gurvich, *Introduction to Physical Chemistry of Crystallophosphors*, Vysshaya Shkola, Moscow, 1982.
27 G. E. Davydyuk, *Non-equilibrium Processes in Semiconductors*, Vezha, Lutsk, 2000.
28 E. Z. Kurmaev, V. M. Cherkashenko and L. D. Finkelnstein, *X-Ray Spectra of Solids*, Nauka, Moscow, 1988.
29 A. Meisel, G. Leonhardt and R. Szargan, *X-Ray Spectra and Chemical Binding*, Springer-Verlag, Berlin/Heidelberg, 1989.
30 Ya. O. Dovgii, I. V. Kityk, M. I. Kolinko, A. S. Krochuk, A. V. Franiv and M. K. Zamorskii, *Phys. Status Solidi B*, 1991, **167**, 637–646.
31 I. V. Kityk, M. I. Kolinko and A. V. Franiv, Ferroelasticity of InI Layered Single Crystals, *Ferroelectrics*, 1992, **130**, 347–350.
32 M. I. Kolinko, I. V. Kityk and A. S. Krochuk, *J. Phys. Chem. Solids*, 1992, **53**(N10), 1315–1320.
33 P. Smok, I. V. Kityk, K. J. Plucinski and J. Berdowski, *Mater. Lett.*, 2002, **56**(3), 364–371.
34 P. Smok, I. V. Kityk, K. J. Plucinski and J. Berdowski, *Phys. Rev. B: Condens. Matter Mater. Phys.*, 2002, **65**, 205103.
35 I. V. Kityk, A. Kassiba, K. J. Plucinski and J. Berdowski, *Phys. Lett. A*, 2000, **265A**, 403–410.
36 A. Brenier, *J. Appl. Phys.*, 2001, **90**(N1), 232–236.